Combustion and Flame 158 (2011) 633–644

Contents lists available at ScienceDirect

Combustion and Flame

journal homepage: www.elsevier.com/locate/combustflame

An improved H_2/O_2 mechanism based on recent shock tube/laser absorption measurements

Zekai Hong, David F. Davidson *, Ronald K. Hanson

Mechanical Engineering Department, Stanford University, Stanford, CA, United States

ARTICLE INFO

Article history:
Received 3 July 2010
Received in revised form 13 September 2010
Accepted 1 October 2010
Available online 30 October 2010

Keywords:
H_2/O_2 mechanism
Laser absorption
Shock tubes
Hydrogen
Oxygen

ABSTRACT

An updated H_2/O_2 reaction mechanism is presented that incorporates recent reaction rate determinations in shock tubes from our laboratory. These experiments used UV and IR laser absorption to monitor species time-histories and have resulted in improved high-temperature rate constants for the following reactions:

$$H + O_2 = OH + O$$

$$H_2O_2(+M) = 2OH(+M)$$

$$OH + H_2O_2 = HO_2 + H_2O$$

$$O_2 + H_2O = OH + HO_2$$

The updated mechanism also takes advantage of the results of other recent rate coefficient studies, and incorporates the most current thermochemical data for OH and HO_2. The mechanism is tested (and its performance compared to that of other H_2/O_2 mechanisms) against recently reported OH and H_2O concentration time-histories in various H_2/O_2 systems, such as H_2 oxidation, H_2O_2 decomposition, and shock-heated H_2O/O_2 mixtures. In addition, the mechanism is validated against a wide range of standard H_2/O_2 kinetic targets, including ignition delay times, flow reactor species time-histories, laminar flame speeds, and burner-stabilized flame structures. This validation indicates that the updated mechanism should perform reliably over a range of reactant concentrations, stoichiometries, pressures, and temperatures from 950 to greater than 3000 K.

1. Introduction

Detailed kinetic mechanisms for the oxidation of hydrocarbons have the H_2/O_2 sub-mechanism as a necessary starting point of their hierarchical structure [1]. This sub-mechanism is critical because it contains many important elementary reactions involving H, O, OH, HO_2, H_2O, and H_2O_2 that play a role in all stages of hydrocarbon oxidation. Continued improvement of the H_2/O_2 sub-mechanism is thus necessary for the continued development and refinement of high-fidelity hydrocarbon mechanisms.

Several detailed kinetic mechanisms dedicated to the H_2/O_2 system have been developed recently [2–6]. In addition to these mechanisms, recent H_2/CO mechanisms [7–10] also contain the corresponding H_2/O_2 sub-mechanisms. While these mechanisms are able to capture the behavior of chemical systems dominated by chain-branching reactions (i.e. ignition delay times), systems dominated by the formation and consumption of HO_2 and H_2O_2 are still subject to relatively large uncertainties. However, work in this area is continuing, and even in the short time since the publication of the H_2/O_2 mechanism by Konnov [6] in 2008, our understanding of H_2/O_2 chemistry, has improved significantly [11–18]. The goal of this study is to develop a mechanism that incorporates these advances in our knowledge.

The current mechanism is tested against shock tube ignition delay times, species profiles obtained in flow reactors, flame speeds, and flame structures. Experimental data for validating the mechanism include those used during the development of earlier mechanisms [4–6]. However, the majority of experimental data previously available for model validation were obtained at low pressures and high temperatures, where the chain-branching reactions dominate and experimental data can be adequately modeled by different parameter sets [6].

Therefore, in order to get a more thorough assessment , the new H_2/O_2 mechanism is compared to experimental data at conditions where, to quote Konnov, "controversial reactions are manifested" [6]. For instance, reactions involving HO_2 and H_2O_2, such as $OH + HO_2 = H_2O + O_2$, H_2O_2 decomposition, and $HO_2 + HO_2 = H_2O_2 + O_2$,

* Corresponding author.
E-mail address: dfd@stanford.edu (D.F. Davidson).

0010-2180/$ - see front matter © 2010 The Combustion Institute. Published by Elsevier Inc. All rights reserved.
doi:10.1016/j.combustflame.2010.10.002

are subject to large uncertainties. These reactions are typically shaded in conventional combustion experiments. Specialized conditions, such as the oxidation of highly diluted hydrogen, the thermal decomposition of H_2O_2 at combustion temperatures, and instantaneously heated H_2O and O_2 mixtures, allow the testing of the rate constants of these reactions in the mechanism. The performance of the current mechanism under these conditions is also compared to that of several other recent mechanisms including Li et al. [4], Ó Conaire et al. [5], Konnov [6], and GRI-Mech 3.0 [19].

2. Reaction mechanism

The improved mechanism (labeled "current mechanism" throughout this paper) is presented in Table 1. The overall reaction scheme is first discussed. This is followed by discussions of several individual reaction rates. Uncertainties for the current rate constants and temperature ranges over which experimental validation exists can be found in Table 1. Pressure dependences are included where appropriate. The proposed mechanism and thermochemical data in CHEMKIN format is included in the Supplemental material.

2.1. Reaction scheme

Before the evaluation of individual reaction rate constants, an overall reaction scheme needs to be chosen. The H_2/O_2 sub-mechanism in GRI-Mech 3.0 [19] has 20 reversible elementary reactions. Later H_2/CO mechanisms by Davis et al. [8] and Sun et al. [10] use the same 20-reaction scheme for H_2 chemistry.

The mechanisms by Li et al. [4], Ó Conaire et al. [5], and the H_2/O_2 sub-mechanism by Sun et al. [10] were premised on the 19-reaction scheme of Mueller et al. [2]. The reaction H + HO_2 = H_2O + O was not included in these three mechanisms, as the authors argued that this reaction is kinetically similar to the reaction H + HO_2 = OH + OH. However, the work by Konnov [6] showed that these two reactions, although not important in slow hydrogen oxidation processes, have opposite signs in laminar flame sensitivities. We have retained the reaction H + HO_2 = H_2O + O in the new H_2/O_2 mechanism.

A 21-reaction scheme was adopted in the Konnov mechanism. The additional reaction is the chain-initiation step $H_2 + O_2$ = OH + OH. As calculations of potential energy surfaces [20] showed that this reaction is highly unlikely, it has not been included in the current H_2/O_2 mechanism. For similar reasons the recent H_2/O_2 chemistry by Williams and co-workers [9] does not include

Table 1
Current H_2/O_2 reaction mechanism. The T range [K] corresponds to the published temperature range of the experimental validation for that reaction rate constant. $k = AT^n\exp(E_a/RT)$ in units of [s^{-1}], [$cm^3mol^{-1}s^{-1}$] or [$cm^6mol^{-2}s^{-1}$].

No.	Reaction	A	n	E_a [cal/mol]	Reference	Uncertainty (±%)	T range [K]
1	H + O_2 = OH + O	1.04E+14		15,286	[11]	10	1100–3370
2	H + O_2 (+Ar) = HO_2 (+Ar)[a]	5.59E+13	0.2	0	[43]	18–35	1050–1250
	Low-pressure limit	6.81E+18	−1.2	0	[43]	–	–
	H + O_2 (+H_2O) = HO_2 (+H_2O)[b]	5.59E+13	0.2	0	[43]	–	–
	Low-pressure limit	3.70E+19	−1.0	0	[43]	–	–
	H + O_2 (+O_2) = HO_2 (+O_2)[a]	5.59E+13	0.2	0	[43]	–	–
	Low-pressure limit	5.69E+18	−1.1	0	[44]	–	–
	H + O_2 (+M) = HO_2 (+M)[a]	5.59E+13	0.2	0	[43]	–	–
	Low-pressure limit	2.65E+19	−1.3	0	[43]	–	–
	Collider efficiency (N_2 = 1): H_2 = 1.5, Ar = 0, H_2O = 0, O_2 = 0		–	–	[44]		
3	H_2O_2 (+M) = 2OH (+M)[c]	8.59E+14		48,560	[14]	21	1000–1200
	Low-pressure limit	9.55E+15		42,203	[12,16]	–	–
	Collider efficiency (Ar = 1): N_2 = 1.5, H_2O = 9		–	–	[12,59,60]		
4	OH + H_2O_2 = H_2O + HO_2	1.74E+12		318	[16]	27	1020–1460
	OH + H_2O_2 = H_2O + HO_2	7.59E+13		7269	[16]	–	–
5	OH + HO_2 = H_2O + O_2	2.89E+13		−500	[15]	27	1600–2200
6	HO_2 + HO_2 = H_2O_2 + O_2	1.30E+11		−1603	[58]		
	HO_2 + HO_2 = H_2O_2 + O_2	4.20E+14		11,980	[58]		
7	H_2O + M = H + OH + M	6.06E+27	−3.31	120,770	[71]		
	Collider efficiency (Ar = 1): H_2O = 0, H_2 = 3, N_2 = 2, O_2 = 1.5				[71]		
	H_2O + H_2O = OH + H + H_2O	1.00E+26	−2.44	120,160	[71]		
8	OH + OH = H_2O + O	3.57E+04	2.4	−2111	[74]	15–25	1050–2380
9	O + H_2 = H + OH	3.82E+12		7948	[45]		
	O + H_2 = H + OH	8.79E+14		19,170	[45]		
10	H_2 + OH = H_2O + H	2.17E+08	1.52	3457	[45]		
11	H + HO_2 = OH + OH	7.08E+13		300	[4]		
12	H + HO_2 = H_2O + O	1.45E+12		0	[45]		
13	H + HO_2 = H_2 + O_2	3.66E+06	2.087	−1450	[20]		
14	O + HO_2 = OH + O_2	1.63E+13		−445	[45]		
15	H_2O_2 + H = HO_2 + H_2	1.21E+07	2.0	5200	[18]		
16	H_2O_2 + H = H_2O + OH	1.02E+13		3577	[45]		
17	H_2O_2 + O = OH + HO_2	8.43E+11		3970	[45]		
18	H_2 + M = H + H + M	5.84E+18	−1.1	104,380	[4]		
	Collider efficiency (Ar = 1): H_2O = 14.4				[4,10]		
	H_2 + H_2 = H + H + H_2	9.03E+14	0	96,070	[45]		
	H_2 + N_2 = H + H + N_2	4.58E+19	−1.4	104,380	[4]		
	H_2 + O_2 = H + H + O_2	4.58E+19	−1.4	104,380	[4]		
19	O + O + M = O_2 + M	6.16E+15	−0.5	0	[29]		
	Collider efficiency (N_2 = 1): H_2 = 2.5, H_2O = 12, Ar = 0				[29]		
	O + O + Ar = O_2 + Ar	1.89E+13	0	−1788	[29]		
20	O + H + M = OH + M	4.71E+18	−1.0	0	[29]		
	Collider efficiency (N_2 = 1): H_2 = 2.5, H_2O = 12, Ar = 0.75				[29]		

[a] F_{cent} = 0.7 [43].
[b] F_{cent} = 0.8 [43].
[c] F_{cent} = 1.

this reaction, though it was included in an earlier mechanism from that group [3].

The reaction O + OH (+M) = HO_2 (+M) is not included in most H_2/O_2 sub-mechanisms [2,4–6,8,10,19], with the exception of two sub-mechanisms by Williams and co-workers [3,9]. A recent study [21] demonstrated that this reaction may impact predictions in lean high-pressure flames. However, given the level of uncertainty in its rate constant (ranging from 10^{15} [22] to 1.2×10^{17} [$cm^6\ mol^{-2}\ s^{-1}$] [23]), this reaction is also not included in the current mechanism. The reaction may be included in future versions of the mechanism once more accurate experimental data become available. In summary, the current mechanism consists of 20 reactions in a form identical to that found in GRI-Mech 3.0; however only five of the reaction rate constants from the GRI-Mech 3.0 mechanism are retained (reactions (6), (8), (10), (15), and (16)).

The thermodynamic data used for the current mechanism are all consistent with the latest database of Burcat [24]. These data include updates to the enthalpy of formation of OH [26,25] and HO_2 [27]. Transport data are not within the scope of the current paper, but can be adapted from JetSurF 1.1 [28], which is the latest version of a detailed chemical reaction model for large hydrocarbon fuels.

2.2. H + O_2 = OH + O (R1)

The chain-branching reaction H + O_2 = OH + O is considered to be one of the most important elementary reactions in combustion and has been studied extensively [11,30–42]; some of these results are plotted in Fig. 1. These studies have produced a consensus [36,38,40–42] for the rate constant (k_1) at temperatures above 1500 K. However, as pointed out by Hwang et al. [42], there still existed large discrepancy among the studies [31,34,35,41] at temperatures near 1100 K. The combined discrepancy in the rate constant at low and high temperatures also implies a discrepancy in the activation energy.

Some previous mechanisms [2–10,18] have relied heavily on the low-temperature data from the H-ARAS (atomic resonance absorption spectroscopy) study by Pirraglia et al. [34]. For example, the Pirraglia et al. expression for k_1 is used directly in the mechanism by Ó Conaire et al. [5]. When compared to laser-based absorption experiments (e.g. [36]), ARAS methods tend to have relatively larger scatter and thus larger experimental uncertainty [31,34,35]. In light of the importance of this chain-branching reaction, a better understanding of the rate constant k_1 at temperatures below 1500 K is needed.

A recent experimental study using tunable diode laser absorption spectroscopy (TDLAS) of H_2O near 2.55 μm has been reported by Hong et al. [11]. The results from this new study agree very well with the Pirraglia et al. study [34], as shown in Fig. 2, as well as with the Masten et al. study (based on laser absorption detection of OH) [36] at the overlapping temperatures. Furthermore, the activation energies for the chain-branching reaction reported by Hong et al. [11] and Masten et al. [36] are within 5%. Hong et al. have recommended an expression, listed in Table 1, based on a combination of the results from these two studies; it is in excellent agreement with the expression recently suggested by Hwang et al. [42] over the entire high temperature window. It should be noted however, as discussed in the original paper by Hong et al. [11], that a major source of uncertainty in k_1 is due to the uncertainty in the rate constant of the reaction H + HO_2 = H_2 + O_2 (k_{13}). Minor adjustments may need to be made to k_1 as more accurate data for k_{13} become available.

2.3. H + O_2 (+M) = HO_2 (+M) (R2)

The chain-terminating reaction H + O_2 (+M) = HO_2 (+M) competes with the major chain-branching reaction H + O_2 = OH + O for H radicals. The low-pressure limit ($k_{2,0}$) of the three-body reaction has been studied in recent years by several groups including Bates et al. [43], Michael et al. [44], and Hwang et al. [42]. A complete review of experimental studies near the low-pressure limit before 2005 can be found in Baulch et al. [45]. The study by Hwang et al. [42] (Ar bath gas) came out after the publication of the Baulch review [45], but their data are well within the quoted uncertainty limits in the Baulch 2005 review.

For a pressure-dependent reaction, it is also important to specify the high-pressure limiting rate constant and fall-off behavior. An early experimental investigation by Cobos et al. [47] studied the rate constant up to 200 atm at room temperature (M = Ar, N_2). However, until recently, only a few high-pressure experimental studies have been reported at elevated temperatures. Hahn et al. [48] studied the rate constant with Ar as the third body at temperatures up to 700 K and pressures up to 900 atm. In 2008, Fernandes et al. [18] extended the Hahn et al. study to three bath gases (Ar, N_2, and He), higher temperatures (up to 900 K), and slightly higher pressures (up to 950 atm). By combining the theoretical high-pressure limiting rate constant ($k_{2,\infty}$ determined from classical trajectory calculations [49]) and low-pressure limiting

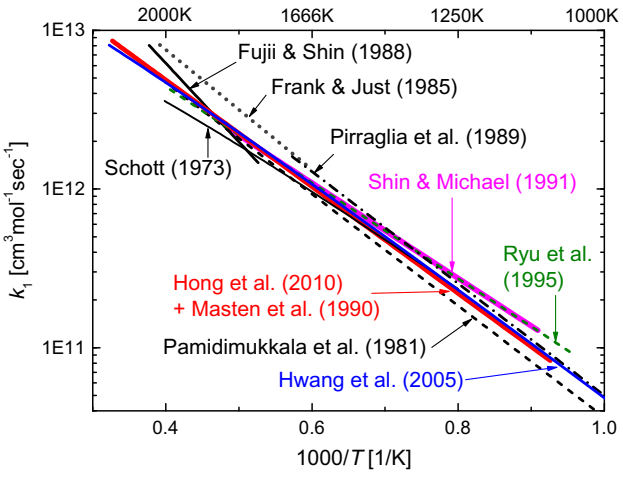

Fig. 1. Arrhenius plot for k_1.

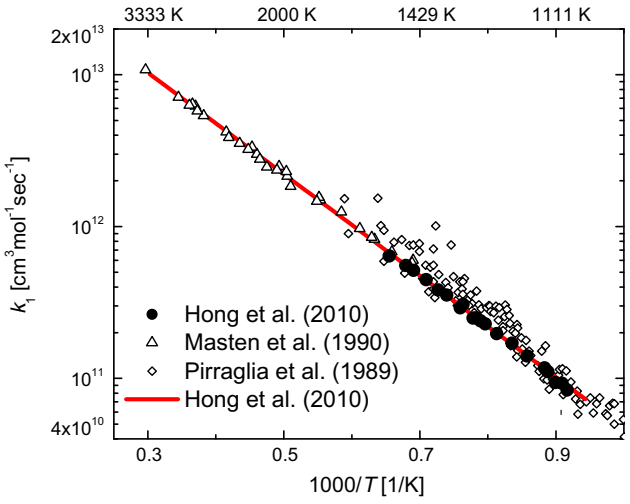

Fig. 2. Arrhenius plot for k_1 with selected experimental data [11, 34, 36].

rate constants ($k_{2,0}$ from the literature [45,44,50,51]) the fall-off behavior was then evaluated. At about the same time, Sellevåg et al. [17] conducted a separate theoretical study for the high-pressure limit and fall-off behavior of the reaction. At higher temperatures, the only direct measurement in the fall-off region was reported by Bates et al. [43]; a few indirect evaluations based on shock tube ignition delay times exist, for example, by Pang et al. [52] and by Mertens et al. [53].

The three recent high-pressure studies (Fernandes et al. [18], Sellevåg et al. [17], and Bates et al. [43]) reported significantly different high-pressure limiting rate constants ($k_{2,\infty}$) and center broadening factors (F_{cent}). However, the differences among the three expressions in the actual rate constant are insignificant below 100 atm, as evidenced by Fig. 3. Miller et al. [46] have pointed out that the deviation from third-body behavior of the reaction under typical combustion conditions is not significant [46] with the exception of supercritical water oxidation. Therefore, the predictive capability of an H_2/O_2 mechanism for typical combustion simulations relies more on the accuracy of $k_{2,0}$ than that of $k_{2,\infty}$ and F_{cent}. Meanwhile, we wish to point out that, as applied combustion problems are moving towards very high pressures, more accurate $k_{2,\infty}$ and F_{cent} data are critically needed to improve the fidelity of combustion mechanisms at these high-pressure conditions [21].

As illustrated by Fig. 4, the discrepancies among k_2 values from different studies basically stem from the differences in $k_{2,0}$ at typical combustion conditions. Because Bates et al. [43] conducted the only direct experimental measurements at high temperature (1050–1250 K), their k_2 expressions, including $k_{2,0}$, $k_{2,\infty}$, and F_{cent}, are adopted in the current mechanisms for M = Ar, N_2, and H_2O. For M = O_2 and H_2, the expressions for the low-pressure limit rate constants are taken from the work by Michael et al. [44].

2.4. H_2O_2 (+M) = 2OH (+M) (R3)

The thermal decomposition of H_2O_2 is regarded as "the central kinetic feature in engine knock in spark ignition engines, in ignition in liquid-fueled diesel engines, and in the operation of homogeneous charge, compression ignition (HCCI) engines" [54], because it is the dominant chain-branching reaction that controls hydrocarbon ignition in the intermediate temperature regime (850–1200 K). Due to experimental challenges, data for this rate constant at temperatures between 1000 and 1200 K, where intermediate temperature hydrocarbon ignition occurs, were only available from one laboratory [55–58]. These have now been supplemented by studies by Hong et al. [12,16].

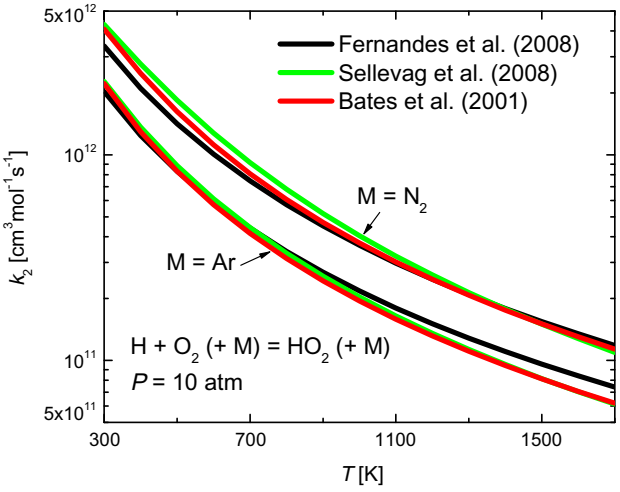

Fig. 4. Arrhenius plot for k_2 at 10 atm. For typical combustion pressures (P < 100 atm), the rate constants are predominantly controlled by the low-pressure limit rate constant of the reaction ($k_{2,0}$).

Hong et al. took a new approach to study this reaction using laser absorption diagnostics for H_2O [12] or for H_2O and OH [16]. As evidenced by Fig. 5, these new data show very good agreement with previous work [58]. In addition, comparing to the previous study, these new results are characterized by significantly reduced scatter and experimental uncertainty (±27% for temperatures higher than 1200 K and ±23% for temperatures between 1000 and 1200 K) [16]. k_3 values near 3.2 atm from Hong et al. [12] are almost indistinguishable from these at lower pressures as illustrated in Fig. 5, and thus are not included in the plot for simplicity. However, there are no existing direct measurements of H_2O_2 decomposition rate constant at much higher pressures for an accurate evaluation of its fall-off behavior [12].

The low-pressure limiting rate constant in Ar bath gas can be specified by $k_{3,0}$ (Ar) = 9.55×10^{15} exp(−21,250 K/T) [cm^3 mol^{-1} s^{-1}] [16] and the collider efficiency of N_2 relative to Ar was estimated to be 1.5 [12]. However, collider efficiencies for other bath gas species were rarely determined by experiments. This could lead to large uncertainty when species other than Ar

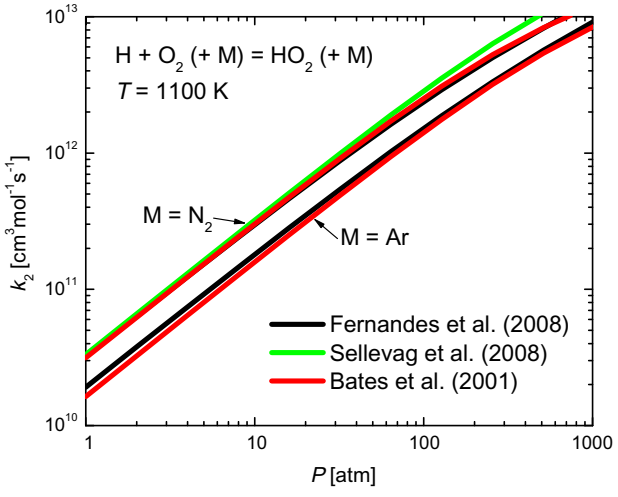

Fig. 3. Variation of the rate constant (k_2) with pressure at 1100 K. Although the rate constant expressions given in the three studies appear different, the differences in the actual rate constants at pressures below 100 atm are insignificant.

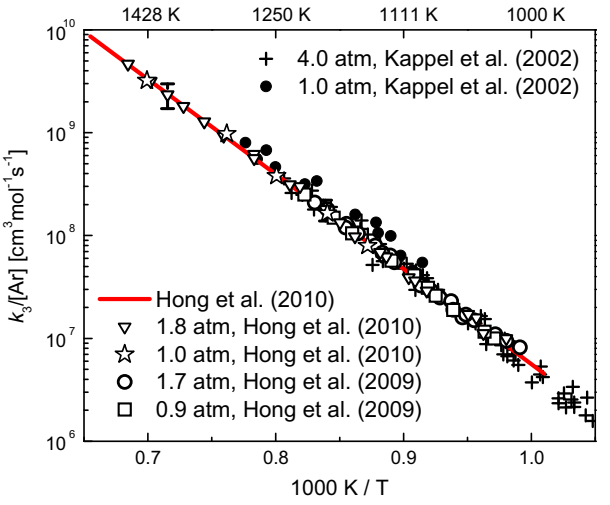

Fig. 5. Arrhenius plot for k_3. Rate constant recommended by Hong et al. and experimental data [12, 16, 58] are shown.

and N_2 are present in large concentrations. In the current mechanism, the O_2 collider efficiency is set equal to that of N_2. Suggested values for the collider efficiencies of H_2O relative to N_2 have been estimated to be 6 or 9 relative to Ar based on early room-temperature studies by Zellner et al. [59] and Forster et al. [60].

Due to the lack of experimental data at high pressures, the current mechanism relies on theoretical studies [13,14] for the high-pressure limiting rate constant ($k_{3,\infty}$). Both theoretical calculations resulted in much larger $k_{3,\infty}$ values than the one recommended by Kappel et al. [58]. The larger $k_{3,\infty}$ values from these two theoretical studies [13,14] are supported by high-pressure studies at room temperature [59,61].

Although the uncertainty in $k_{3,\infty}$ is relatively large as a result of the lack of high-pressure experimental data, it should be noted that, for most combustion applications, the predictive power of a mechanism is determined mostly by the accuracy of $k_{3,0}$. The reason is that the deviation from the low-pressure limiting behavior of the H_2O_2 thermal decomposition reaction is insignificant under typical combustion conditions, similar to the argument presented for the chain-terminating reaction $H + O_2$ (+M) = HO_2 (+M). For the same reason, the recent experimental results reported at low pressures [12,16] are heavily weighted in the current mechanism. Therefore, we choose to use $F_{cent} = 1$ to accurate represent these low-pressure experimental data [12,16].

However, one has to realize that $k_{3,\infty}$ and F_{cent} approximations made during the development of this mechanism are compromises we have to make in face of the lack of reliable experimental data at high pressures. This could be remedied once accurate experimental data at high pressures become available.

2.5. $OH + H_2O_2 = H_2O + HO_2$ (R4)

Because of the difficulty in detecting H_2O_2 and HO_2, there are fewer studies of reactions of these species. In earlier mechanisms, the rate constants for the reaction $OH + H_2O_2 = H_2O + HO_2$, k_4 were derived from studies by Hippler et al. [62,63]. However, a recent study in our laboratory [16] of the rate constant k_4 should provide an improved rate constant expressions for k_4 over that used in previous mechanisms [10,4–6,19]. The new results are presented in Fig. 6.

The current mechanism uses a k_4 rate constant recommended by Hong et al. [16] that is the sum of two Arrhenius expressions that they derived by combining their high-temperature data with previous studies at low to intermediate temperatures (refer to [16] for references):

$$k_4 = 1.74 \times 10^{12}\ \exp(-160\ \mathrm{K}/T) + 7.59 \times 10^{13}\ \exp(-3660\ \mathrm{K}/T)\ [\mathrm{cm^3\ mol^{-1}\ s^{-1}}]$$

This recommended expression for k_4 is plotted in Fig. 6 as the red curve. It should be noted that currently, to the knowledge of the authors, no experimental data exist between 500 and 1000 K, where some groups have suggested that a significant change in the activation energy could exist. Further experimental data are needed to confirm this possible transition in activation energy.

2.6. $OH + HO_2 = H_2O + O_2$ (R5)

The rate constant of the reaction $OH + HO_2 = H_2O + O_2$ (k_5) probably has the largest uncertainty (of the 20 reaction rate constants) among the comparative mechanisms, as evidenced by Fig. 7. This is because of the unusual behavior reported by previous researchers. Hippler et al. [63] found a deep and unusually narrow rate constant minimum close to 1250 K. Kappel et al. [58] later reported a similar rate constant minimum, but at a notably shifted temperature near

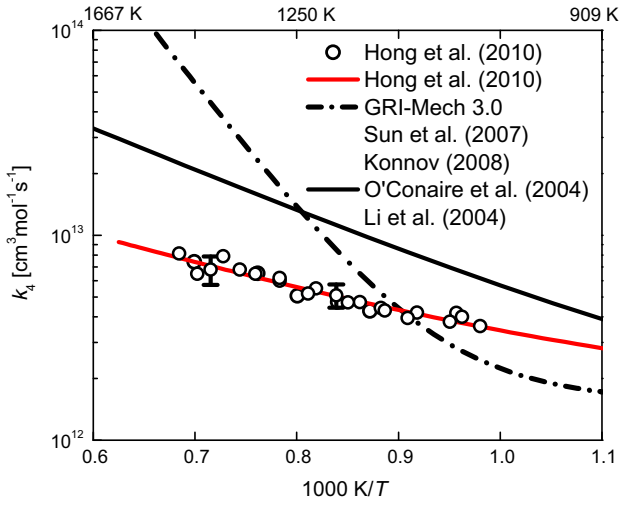

Fig. 6. Arrhenius plot for k_4. Previous studies [4–6, 10, 19] and the experimental data and recommended rate constant (in red) from Hong et al. [16] are shown. Rates for GRI-Mech 3.0, Sun et al. and Konnov are the same, as are the rates for Ó Conaire et al. and Li et al. (For interpretation of the references to color in this figure legend, the reader is referred to the web version of this article.)

1000 K. Both studies suggest that the reaction rate constant has a strong temperature dependence at high temperatures.

Srinivasan et al. [64] experimentally studied k_5 and reported an average value for $k_5 = (4.0 \pm 1.6) \times 10^{13}$ [cm^3 mol^{-1} s^{-1}] between 1237 and 1554 K. However, the experimental scatter prevented these authors from drawing a strong conclusion about the temperature dependence of the reaction rate constant. Very recently, Hong et al. [15] investigated the reaction in its reverse direction. The new study clearly shows that the strong temperature dependency of k_5 assumed in some mechanisms [6,8,19] does not exist between 1600 and 2200 K, and that k_5 can be well-represented by $(3.3 \pm 0.9) \times 10^{13}$ [cm^3 mol^{-1} s^{-1}]. This latest study is in good agreement with Srinivasan study [64]. These two recent studies, together with studies at low temperatures [65–68], support a value of

$$k_5 = 2.89 \times 10^{13}\ \exp(252/T)\ [\mathrm{cm^3\ mol^{-1}\ s^{-1}}]$$

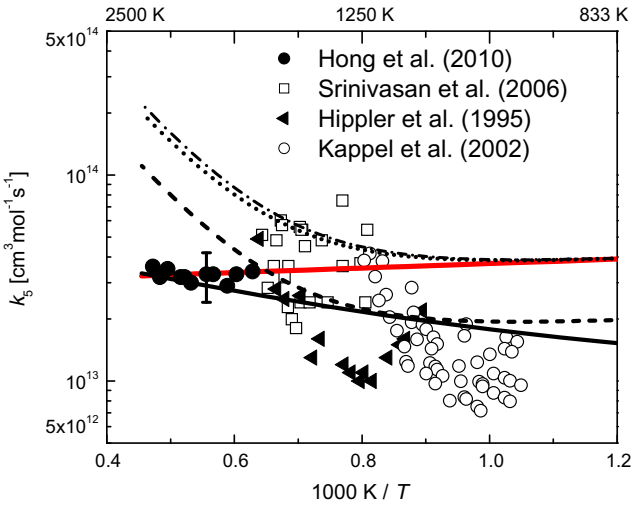

Fig. 7. Arrhenius plot for k_5. Curves are k_5 expressions adopted in some representative mechanisms (red solid: Baulch et al. [69,70], also used by Mueller et al. [2], Li et al. [4], and Ó Conaire et al. [5]; black solid: Sun et al. [10]; dot: Konnov [6]; short dash: GRI-Mech 3.0 [18]; dash dot: Davis et al. [8]). (For interpretation of the references to color in this figure legend, the reader is referred to the web version of this article.)

that was recommended in early Baulch et al. reviews [69,70] and is used in the current mechanism. As Hong et al. [15] pointed out, caution should be exercised when using the above k_5 expression between 400 and 1200 K, because a rate constant minimum may possibly exist near 1250 K [63] or 1000 K [58].

2.7. $H_2O + M = H + OH + M$ (R7)

In most previous mechanisms [4,5,9,3,7,10,8,18], this reaction was expressed in the recombination direction. Recently, Srinivasan and Michael [71] studied the thermal decomposition of H_2O between 2196 and 2792 K and reported a rate constant for the decomposition direction. Their new expression is adopted in the current mechanism and the mechanism by Konnov [6]. The uncertainty of the Srinivasan and Michael study was estimated by the authors to be ±18%. However, as pointed out by Konnov [6], there also exist data [72,73] that are systematically lower than other literature values by a factor of 4–5. As a result, the uncertainty of the reaction rate constant was estimated to be a factor of 2 by Konnov.

It is also noticed that the description of the fall-off behavior of the reaction $H_2O + M = H + OH + M$ was purposely omitted in previous mechanisms, for the reason that the deviation from the low-pressure limiting rate is insignificant under typical combustion conditions. A theoretical study has been recently carried out to investigate the reaction's pressure dependence and its high-pressure limiting rate [17]. Using $k_{7,\infty}$, and F_{cent} given in the literature [17], it appears that the second-order rate constant expression is satisfactorily accurate in describing the kinetics of this reaction under typical combustion conditions. In light of the level of uncertainty that exists in $k_{7,0}$, use of a second-order rate constant for H_2O thermal decomposition is deemed sufficient and is thus retained in the current mechanism.

2.8. $2OH = H_2O + O$ (R8)

The rate constant of the reaction $2OH = H_2O + O$ (k_8) was measured by Wooldridge et al. [74] in our laboratory with estimated uncertainties of −16% to +11% at $T > 2100$ K and −22% to +25% at $T = 1050$ K. The reaction has also been studied in the reverse direct $O + H_2O \rightarrow 2OH$ (k_{-8}) by the Brookhaven group in 1991 [75,76]. Using the updated OH heat of formation [25,26], k_{-8} can be converted to $k_8 = 4.34 \times 10^3\ T^{2.7} \exp(951/T)$ [cm^3 mol^{-1} s^{-1}], in good agreement with the Wooldridge expression $k_8 = 3.57 \times 10^4\ T^{2.40} \exp(1063/T)$ [cm^{3}mol^{-1}s^{-1}] [74]. A reevaluation of k_8 by Hong et al. [16] is in excellent agreement with the two aforementioned expressions. The rate expression of Wooldridge et al. [74] is used in the current mechanism.

2.9. Other reactions

Other rate constants are identical to those suggested by GRI-Mech 3.0 [18] (reactions (6), (8), (10), (15), and (16)) or from the review by Baulch et al. [45] (reactions (9), (10), (12), (14), (16), and (17)). As discussed in the introduction section, Konnov [6] has pointed out that it may be necessary to include all three product channels of the reaction between H and HO_2 ($H + HO_2 = 2OH$; $H + HO_2 = H_2O + O$; and $H + HO_2 = H_2 + O_2$).

In particular, reactions $H + HO_2 = 2OH$ and $H + HO_2 = H_2 + O_2$ have been demonstrated [4,5] to be important in capturing species time-histories from flow reactor studies and laminar flame speeds. However, knowledge of these two rate constants is very limited. The only known set of near-direct experiments of the reaction $H + HO_2 = H_2 + O_2$ at combustion temperatures was performed by Michael et al. [20] by studying the reverse initiation reaction $H_2 + O_2 = H + HO_2$ between 1662 and 2097 K. Using the equilibrium constant, forward rate constants (k_{13}) can be calculated from data

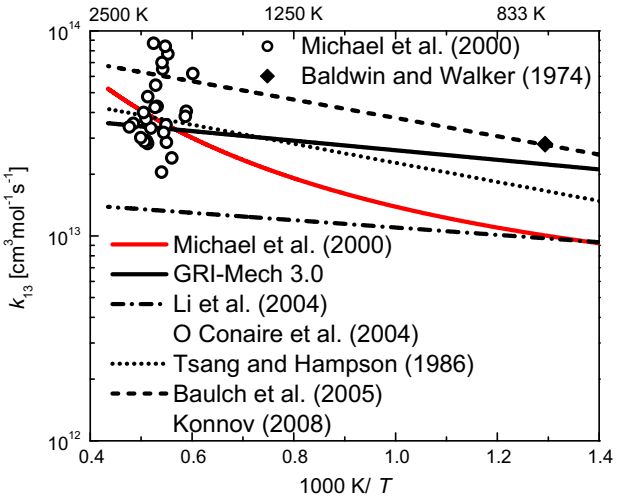

Fig. 8. Arrhenius plot for k_{13}. Curves are k_{13} expressions proposed in some previous mechanisms or reviews (red solid: Michael et al. [20]; black solid: GRI-Mech 3.0 [18]; dash dot: Li et al. [4], also used by Ó Conaire et al. [5]; dot: Tsang and Hampson [29]; short dash: Baulch et al. [45], also used by Konnov [6]). (For interpretation of the references to color in this figure legend, the reader is referred to the web version of this article.)

reported by Michael et al. [20] in the reverse direction (k_{-13}) and are plotted in Fig. 8. In the same plot, a k_{13} value at 773 K inferred from an early flame study by Baldwin and Walker [77] is also presented. For simplicity, experimental results near room temperature [78–81] are not shown in the same figure. Michael et al. [20] recommended an expression for k_{-13} based on their experimental and theoretical studies, which leads to $k_{13} = 3.66 \times 10^6\ T^{2.087} \exp(730/T)$ [cm^{3}mol^{-1}s^{-1}] if the equilibrium constant given in the same study [20] is utilized for the conversion. This k_{13} expression is adopted in the current mechanism, see the red curve in Fig. 8.

We have used the same expression for the rate constant of the reaction $H + HO_2 = 2OH$ as that in the Li et al. [4] mechanism, that mechanism shows good agreement with currently available data from flow reactor studies and laminar flame speed measurements. The rate constants for the third product channel $H + HO_2 = H_2O + O$ are taken directly from the evaluation by Baulch et al. [45].

3. Results and discussion

3.1. Validations against specialized data

The goal of this section is to validate the current mechanism at conditions where "'controversial' reactions are manifested" [6] or important reactions are isolated. To achieve this goal, some specialized conditions have to be exploited, for instance, the study of H_2 oxidation in extremely diluted mixtures. In addition to investigations of H_2 ignition (oxidation), other combinations of species containing only H and/or O elements, for example, H_2O_2 and H_2O, provide unique opportunities to test and validate the H_2/O_2 mechanism. In the following examples, comparisons will be made with simulations based on the current mechanism and those of Li et al. [4], Ó Conaire et al. [5], Konnov [6], and GRI-Mech 3.0 [19].

3.1.1. H_2 oxidation in extremely dilute mixtures

Both H_2O and OH time-histories have been reported during H_2 oxidation in extremely dilute mixtures [11,36]. H_2 ignition delay times are strongly susceptible to impurities [11], whereas the rapid rise of the slope of both the H_2O and OH profiles at ignition is not significantly affected by impurities. Therefore, the relative shapes

of these profiles, instead of the absolute time scales, are valuable kinetic targets for validating the H_2/O_2 sub-mechanisms.

In Figs. 9 and 10, experimental H_2O time-histories [11] recorded at 1472 K and 1100 K, respectively, are compared to model predictions. Trace amounts of H-atoms (at sub-ppm levels) are included as reactants in the CHEMKIN inputs to simulate impurity effects, and thus allow the ignition delay times to be matched very accurately. Alternatively, the simulations can be shifted slightly in time to match the ignition delay times. At 1100 K, the current mechanism and GRI-Mech 3.0 [19] accurately simulate the H_2O time-histories, whereas other mechanisms are not as successful.

At higher temperatures, OH time-histories have been reported [36] and are used to validate the current mechanism. Figure 11 compares data and simulations of OH time-history during the oxidation of H_2 at 1980 K and 0.675 atm in a fuel-rich H_2/O_2/Ar mixture (0.493% O_2, 5% H_2, balance Ar). Experimental data (in blue) are from Masten et al. [36]. Due to small uncertainties in the OH absorption cross-section and the mixture compositions, the OH profiles were treated as self-calibrating by matching the plateau values in the original work of Masten et al. [36]. We took the same approach by re-scaling calculated OH profiles to match the experimental OH plateau. Only the current mechanism and the latest Konnov mechanism [6] closely match these experimental data.

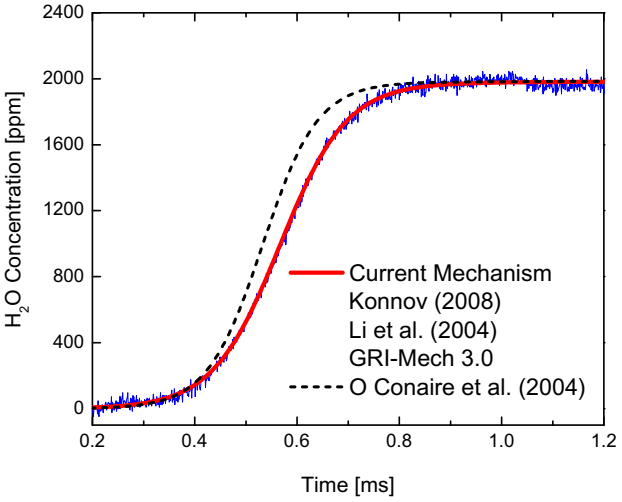

Fig. 9. H_2O time-history during the oxidation of H_2 at 1472 K and 1.831 atm in a fuel-rich H_2/O_2/Ar mixture (0.1% O_2, 0.9% H_2, balance Ar). Experimental data (in blue) are from Hong et al. [11]. A reference has indistinguishable predicted species time-history as the one above it with a legend, if there is no legend next to the reference (same thereafter). (For interpretation of the references to color in this figure legend, the reader is referred to the web version of this article.)

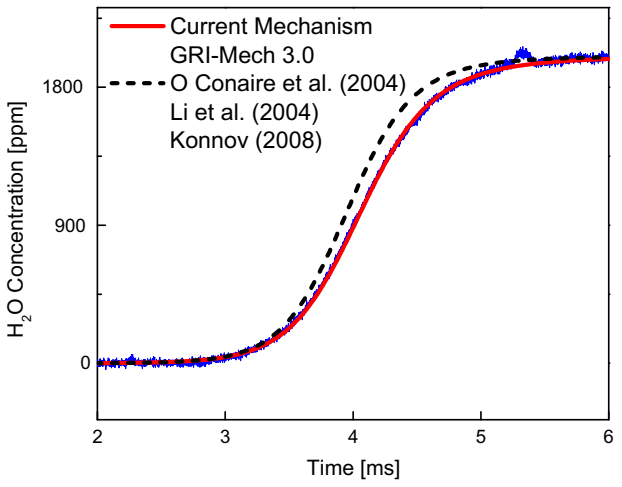

Fig. 10. H_2O time-history during the oxidation of H_2 at 1100 K and 1.953 atm in a fuel-rich H_2/O_2/Ar mixture (0.1% O_2, 2.9% H_2, balance Ar). Experimental data (in blue) are from Hong et al. [11]. (For interpretation of the references to color in this figure legend, the reader is referred to the web version of this article.)

3.1.2. H_2O_2 thermal decomposition

The thermal decomposition of H_2O_2 provides a unique opportunity to test and validate rate constant values for isolated H_2O_2/HO_2 reactions. Both H_2O and OH time-histories have been reported recently by Hong et al. [12,16]. In Figs. 12 and 13, experimental data recorded at initial reflected shock conditions of 1192 K, 1.95 atm with 2216 ppm initial H_2O_2 are compared to mechanism predictions. The H_2O profiles predicted by Li et al. [4], Ó Conaire et al. [5], and GRI-Mech 3.0 [19] are almost indistinguishable and are represented by one single curve in Fig. 12. The current mechanism has the best performance among all the mechanisms tested.

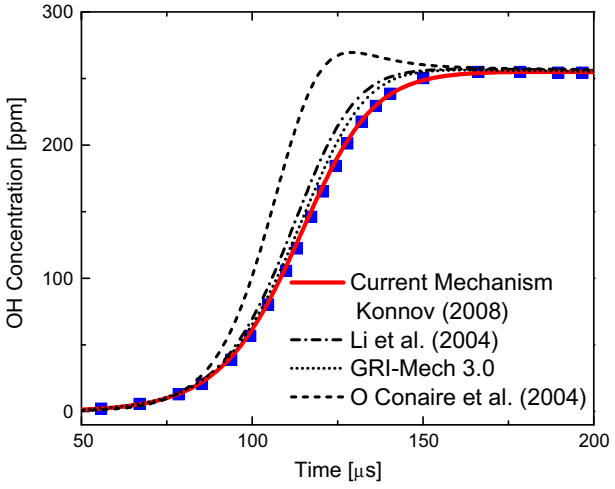

Fig. 11. OH time-history during the oxidation of H_2 at 1980 K and 0.675 atm in a fuel-rich H_2/O_2/Ar mixture (0.493% O_2, 5% H_2, balance Ar). Experimental data (in blue) are from Masten et al. [36]. (For interpretation of the references to color in this figure legend, the reader is referred to the web version of this article.)

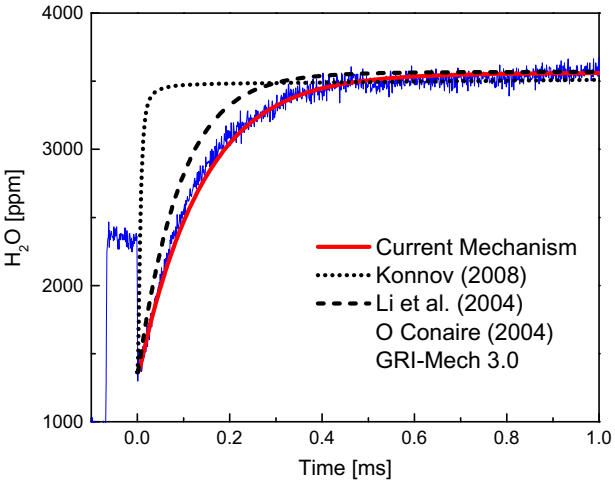

Fig. 12. H_2O time-history during the thermal decomposition of H_2O_2 at 1.95 atm, 1192 K. Test mixture: 2216 ppm H_2O_2/1364 ppm H_2O/682 ppm O_2/Ar. Experimental data (in blue) are from Hong et al. [16]. (For interpretation of the references to color in this figure legend, the reader is referred to the web version of this article.)

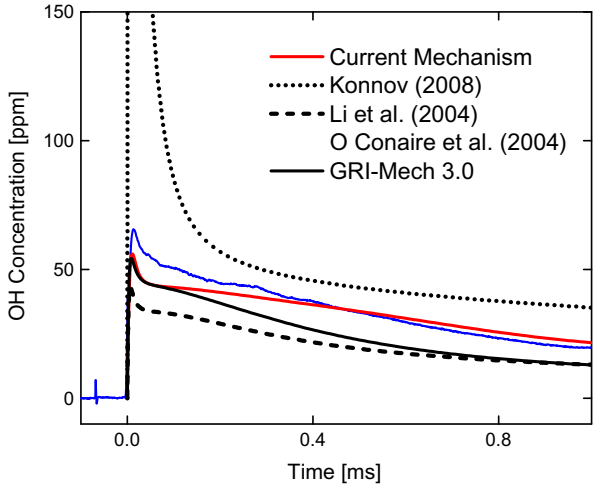

Fig. 13. OH time-history during the thermal decomposition of H_2O_2 at conditions of those of Fig. 12. Experimental data (in blue) are from Hong et al. [16]. (For interpretation of the references to color in this figure legend, the reader is referred to the web version of this article.)

The OH time-history presented in Fig. 13 was measured simultaneously with the H_2O profile shown in Fig. 12. Again, the best agreement is seen with the current mechanism. Other mechanisms (Li et al. [4], Ó Conaire et al. [5], and GRI-Mech 3.0 [19]), although they overpredict the rate of H_2O_2 thermal decomposition (Fig. 12), under-predict the peak OH values. This opposite effect is attributed to the larger rate constant (than that recommended here) used in these mechanisms [4,5,19] for reaction (4) OH + H_2O_2 = H_2O + HO_2.

Comparisons between experimental H_2O/OH time-histories and model predictions are also made at a much higher temperature (1498 K). These comparisons lead to results similar to those of the 1192 K case discussed above (see Supplemental materials).

3.1.3. High-temperature H_2O/O_2 reaction

Another environment that provides opportunities for improving the understanding of H_2/O_2 reactions is the high-temperature H_2O/O_2 system. Representative OH time-histories have been reported in shock-heated H_2O/O_2/Ar mixtures [15]. A sample OH profile is shown in Fig. 14 for a reflected shock wave experiment with a mixture consisting of 1.3% H_2O, 0.99% O_2, balance Ar at 1880 K and 1.74 atm. The current mechanism and the Li et al. [4] and Ó Conaire et al. [5] mechanisms all reproduce the experimental OH time-history with good accuracy and are indistinguishable in Fig. 13.

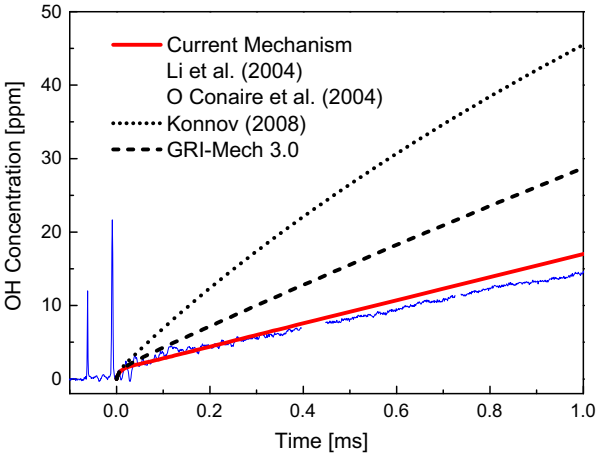

Fig. 14. OH time-history in a shock-heated 1.3% H_2O/0.99% O_2/97.71% Ar mixture. Initial reflected shock conditions: 1880 K, 1.74 atm. Experimental data (in blue) is from Hong et al. [15]. (For interpretation of the references to color in this figure legend, the reader is referred to the web version of this article.)

3.2. Validations against conventional combustion data

In addition to validating the current mechanism at specialized reaction conditions, the mechanism is also validated against experimental data obtained under more conventional combustion conditions. These include ignition delay times in shock tubes, species time-histories in flow reactors, unstretched laminar flame speeds, and burner-stabilized flame structures.

These more conventional data have been studied extensively in the development of previous models [2,4–6,8]. Almost all these models have achieved good agreement with these experimental data, and for simplicity, these comparisons are not included in these discussions.

3.2.1. Shock tube ignition delays

Shock tube ignition delay times are widely used for the calibration of combustion mechanisms at intermediate to high temperatures (T > 1000 K). H_2 ignition delay behavior has been extensively studied by previous researchers, for example see references [52,82–87]. The recent shock tube study of H_2 ignition delay times by Pang et al. [52] provides a unique opportunity for the validation of the current mechanism, because the Pang et al. [52] study reported the facility-related non-ideal pressure rise as a function of time. This enables a more accurate simulation of ignition behavior.

Li et al. have developed a method, CHEMSHOCK, to account for the effects of non-ideal pressure rise behind reflected shock waves by using the experimentally-measured pressure time-history (up to the time of ignition) as a constraint on the calculation [88]. Using this method, the ignition delays times from Pang et al. [52] are compared to the predictions made by the current mechanism in Fig. 15 using dP^*/dt = 2%/ms ($P^* = P/P_0$, where P_0 is the initial post-reflected-shock pressure). The comparison shows excellent agreement over the entire temperature range studied by Pang et al. [52]. Ignition delay predictions made with a constant energy–volume (U–V) approximation, also using the current mechanism, are contrasted in the same plot. The discrepancy between

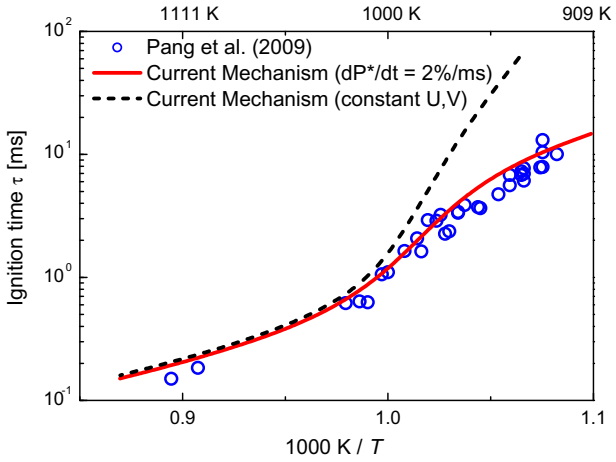

Fig. 15. Ignition delay times predicted by the current mechanism, by assuming either a constant U–V reactor (CHEMKIN) or a reactor with a pressure rises at a rate of 2%/ms (CHEMSHOCK). The experimental data (in blue) are from Pang et al. and are for mixtures of 4% H_2, 2% O_2, balance Ar at 3.5 atm [52] with an experimental facility-related pressure rise of 2%/ms. (For interpretation of the references to color in this figure legend, the reader is referred to the web version of this article.)

the two approaches (constant U–V and time-varying pressure) becomes significant at long ignition delay times ($\tau > 1$ ms).

In addition to the experimental investigation discussed above, ignition delay times were also studied at elevated pressures, at different equivalence ratios (ϕ), and with various bath gases, such as N_2 and H_2O [82–87]. The predictions using the current mechanism consistently enjoy good agreement with these experimental data. Comparisons with these data are presented in the Supplemental materials.

3.2.2. Species time-histories from flow reactors

Flow reactors enable combustion to be studied at intermediate temperatures (typically below 1200 K), where hydrogen peroxide and hydroperoxyl reactions can be important. Although recent studies [12,15,16] have significantly improved the understanding of these reactions, the rate constants of some of the reactions still lack the support of consistent experimental data. For example, the reactions $H + HO_2 = 2OH$ and $H + HO_2 = H_2 + O_2$ are subject to large uncertainties as evidenced by the recent review of Baulch et al. [45]. Due to the uncertainties in the rate constants of these reactions, flow reactor experiments at intermediate temperatures provide some of the most valuable data for hydrogen mechanism validation [6].

A common approach for converting experimental profiles as a function of axial distance into time profiles is to shift the calculated time-histories to match the points where 50% of a major reactant is consumed [2]. This approach is used in the present study to make comparisons between experimental data and simulations using the current mechanism. In addition, an adiabatic process is usually assumed to model combustion in flow reactors, although heat losses cannot be completely eliminated. As shown in Fig. 16, the adiabatically calculated exhaust gas temperature is slightly higher (~5 K) than measurements. Previous studies have shown that differences in species time-histories are minor if the experimentally measured temperature profile is used instead of the adiabatically calculated one [2,6]. For simplicity, species time-histories are calculated with the adiabatic assumption (shown as curves) in the current study and compared to experimental data.

The experimental data presented in Fig. 16 were taken at 880 K, 0.3 atm, with 0.5% H_2 and 0.5% O_2 diluted in N_2 by Mueller et al. [2]. After shifting all calculated curves (species time-history and temperature) forward by 0.071 s, the simulations compare favorably with the experimental data. The mechanism is also validated against flow reactor data over a range of equivalence ratios ϕ, temperatures, and pressures. For instance, H_2 mole fraction profiles were experimentally measured at $\phi \approx 0.5$, 6.5 atm, and over a temperature range of 884–934 K [2], as shown in Fig. 17. The comparisons at all temperatures show excellent agreement. Further mechanism validations against flow reactor data can be found in the Supplemental materials.

3.2.3. Unstretched laminar flame speeds

The speed of freely propagating flames (s_u^o) can be studied as a function of equivalence ratio, temperature, pressure, and dilution. Using the concept first suggested by Wu and Law [89], experimentally-measured flame speeds, either in counter-flow burners or in constant-volume bombs, must be corrected for flame stretch effects. Figure 18 provides measured and simulated results for the unstretched laminar flame speed at standard initial temperature and ambient pressure, as a function of equivalence ratio of mixtures with N_2 and Ar as diluents. The mole ratio between O_2 and diluents was fixed at 1:3.76. In the case of N_2 diluent, the O_2/N_2 mixture is essentially that of air.

The data in Fig. 18 are taken from various literature sources [89–93]. The curves are the predictions made with the current mechanism using the "Flame Speed Calculator" model of CHEMKIN-PRO [94]. The flame speed calculations are repeated until the temperature and species slopes at the boundaries are close to zero and both gradient and curvature controls are less than 0.1.

As evident in Fig. 18, the agreement between experimental data and model predictions are very good for both diluents at a moderate dilution ratio (O_2:diluent = 1:3.76), standard temperature (unburnt mixtures), and ambient pressure. Experimental studies have also been reported when a more diluted oxidizer mixture (O_2:N_2 = 1:12) was used at the standard temperature and pressure [95,96]. At these conditions, the current mechanism predicts unstretched flame speeds that agree with experimental data [95,96], as presented in Fig. 19.

Recently, Burke et al. [21] studied the mass burning rate (f^o) of H_2 flames at pressures up to 25 atm, where f^o is defined as the product of the unburnt gas density (ρ_u) and unstretched laminar flame speed (s_u^o). Negative pressure dependence of mass burning rates was found for H_2/O_2/Ar flames of equivalence ratio 2.5 [21], whereas all mechanisms tested in the Burke et al. study [21] either could not fully capture the negative pressure dependence [4–6,8,9] or under-predict mass burning rates [10,19]. As presented in

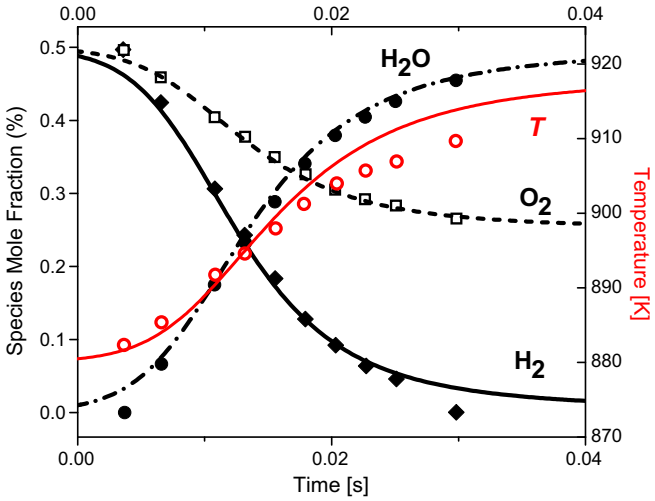

Fig. 16. Species profiles from a flow reactor experiment [2]. The unburnt mixture was at 880 K, 0.3 atm and comprised of 0.5% H_2, 0.5% O_2, with the balance N_2. The curves are calculated with the current mechanism using an adiabatic approximation. All calculated curves are simultaneously shifted forward by 0.071 s.

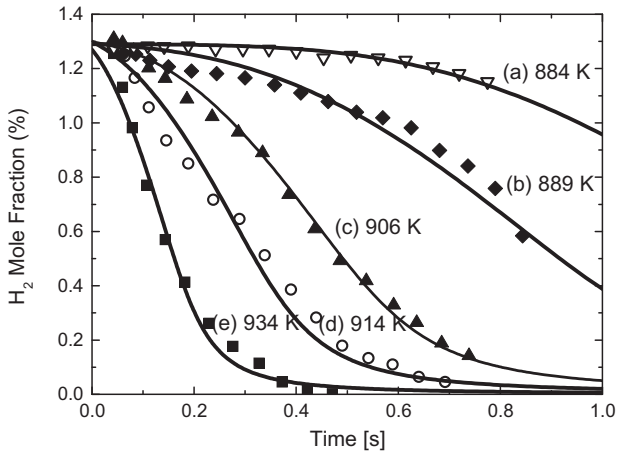

Fig. 17. H_2 mole fractions recorded at 6.5 atm and at various initial temperatures [2]. The unburnt mixtures were: (a) 1.29% H_2/2.19% O_2/N_2, time shifted forward by 0.30 s; (b) 1.30% H_2/2.21% O_2/N_2, time shifted forward by 0.54 s; (c) 1.32% H_2/2.19% O_2/N_2, time shifted forward by 0.40 s; (d) 1.36% H_2/2.24% O_2/N_2, time shifted forward by 0.38 s; (e) 1.36% H_2/2.24% O_2/N_2, time shifted forward by 0.24 s. Curves are calculated using the current mechanism and an adiabatic reactor.

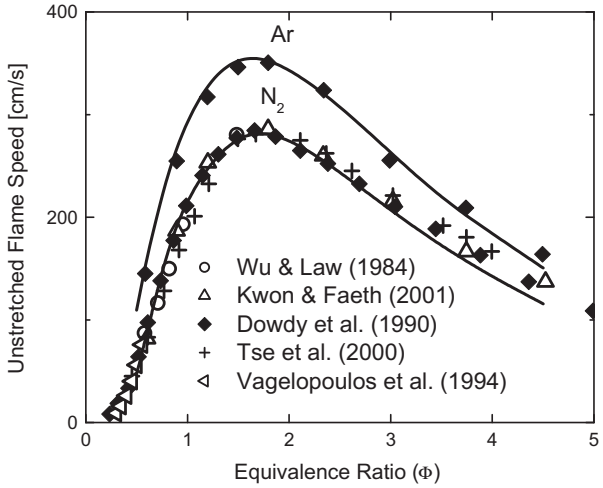

Fig. 18. Laminar flame speed for H_2/O_2 diluted in N_2 and Ar at 1 atm. The mole ratio between O_2 and diluent (Ar, N_2) is 1:3.76. Experimental data are from Refs. [89–93]; the curves are the predictions using the current mechanism.

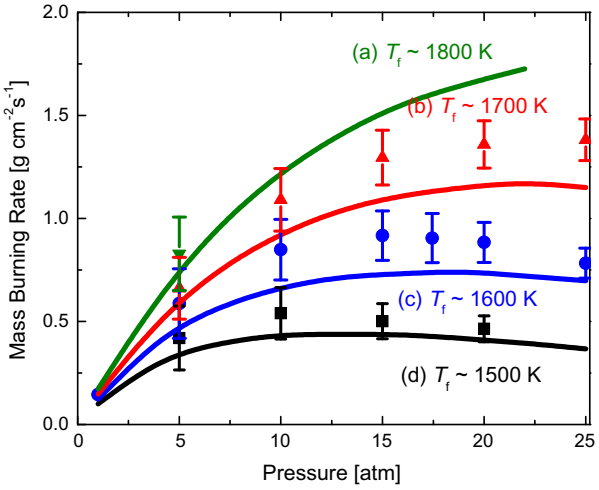

Fig. 20. Mass burning rates of $H_2/O_2/Ar$ flames of equivalence ratio 2.5 at various nominal flame temperatures (T_f). The unburnt mixtures were: (a) $T_f \sim 1800$ K, 38.46% H_2/7.69% O_2/Ar; (b) $T_f \sim 1700$ K, 35.21% H_2/7.04% O_2/Ar; (c) $T_f \sim 1600$ K, 32.21% H_2/6.44% O_2/Ar; (d) $T_f \sim 1500$ K, 29.41% H_2/5.88% O_2/Ar. Curves are calculated using the current mechanism; data are from Burke et al. [21].

Fig. 20, the current mechanism accurately captures the negative pressure dependence of mass burning rates at various nominal flame temperatures (T_f). In addition, the overall agreement between the current mechanism predictions (curves) and experimental data (scatters and error bars) is good. Further improvements of the mechanism may require a better understanding of reactions involving HO_2, such as $H + O_2 (+M) = HO_2 (+M)$, $H + HO_2 = H_2 + O_2$, and $H + HO_2 = 2OH$ [21].

3.2.4. Burner-stabilized flame structure

Burner-stabilized flame structures reported in the literature can also be used to validate the current mechanism. The "Premixed Burner" model of CHEMKIN-PRO [94] is used in the present study to carry out calculations. A set of experimental data that is widely used for the validation of H_2 mechanisms is from the work by Dixon-Lewis et al. [98] (Fig. 21). The study used a fuel-rich $H_2/O_2/N_2$ mixture (mole fraction: 18.83% H_2, 4.60% O_2, balance N_2). The unburnt gas was at 336 K and 1 atm, with the calculated adiabatic flame temperature of 1078 K. The experimentally measured burning velocity was 9.2 ± 0.2 [cm/s] referring to unburnt gas at 291 K. To account for heat losses in the burner flame, the temperature profile is specified using the experimental data reported in the same work [98]. In Fig. 21, the comparisons are made between species profiles as functions of distance above the burner surface. Note that the species mole fractions are normalized by N_2 mole fraction, as presented in the original work [98]. Very good agreement between the model predictions and experimental data are found.

A more recent study conducted using a low pressure (0.047 atm) burner was reported by Vandooren and Bian [99] using molecular beam sampling and mass spectrometry (MBMS). The reactant mixture was composed of 39.7% H_2, 10.3% O_2 and balance Ar (by mole). The experimentally measured burning velocity was 131 [cm/s] referring to unburnt gas. Both the experimental data and simulations using the current mechanism are shown in

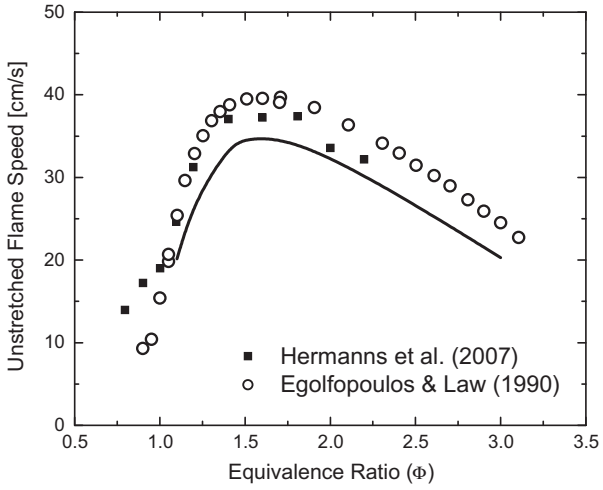

Fig. 19. Laminar flame speed in very diluted $H_2/O_2/N_2$ mixtures (O_2:N_2 = 1:12) with unburnt mixtures at standard temperature and pressure. Experimental data are from references [96,97] and the curve is calculated using the current mechanism.

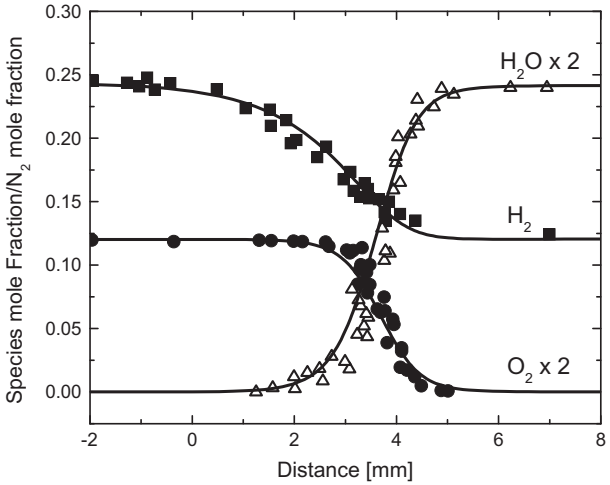

Fig. 21. Species spatial profiles obtained from a burner-stabilized flame structure study [98]. The species profiles were normalized using N_2 mole fraction. The unburnt mixture consisted of 18.83% H_2 and 4.60% O_2 (balance N_2) and was at 336 K and 1 atm. The temperature profile that is used for simulation is taken from the same study [98]. Solid lines: simulations using the current mechanism.

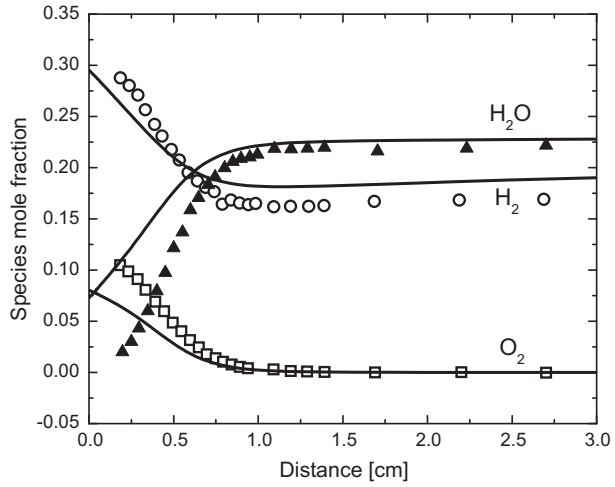

Fig. 22. The structure of a burner-stabilized flame studied using a mixture of 39.7% H_2, 10.3% O_2 and balance Ar (by mole) at 0.047 atm. Experimental data are from the study by Vandooren and Bian [99]; the curves are calculated using the current mechanism.

Fig. 22, and are in reasonable agreement with each other. Similar to what has been reported by Ó Conaire et al. [5], there is some discrepancy between experimental data and model predictions in the close vicinity of the burner surface. More accurate simulations of species profiles will likely require that radical quenching on the burner surface be properly included [5].

In addition to the flame structures obtained at ambient or lower pressures, burner-stabilized flame structure has also been studied at an elevated pressure (10 atm) by Paletskii et al. [100]. The comparison between these experimental data and the model predictions yields reasonable good agreement (presented in the Supplemental materials). However, at this elevated pressure, the flame front thickness is only 0.7 mm, whereas the claimed spatial resolution of the probe was approximately 0.1 mm. As pointed out by Konnov [6], the more gradual changes in the experimental profiles may be a result of the spatial averaging effects by the probe.

4. Conclusions

A new H_2/O_2 reaction mechanism has been proposed that incorporates recent reaction rate determinations using shock tube/laser absorption from our laboratory, as well as recent studies from other laboratories. These shock tube/laser absorption measurements offer more accurate rate constants for several important reactions including $H + O_2$, H_2O_2 decomposition, and the reaction of OH with H_2O_2 and HO_2. The new mechanism has been tested against OH and H_2O species time-histories in various H_2/O_2 systems, such as H_2 oxidation, H_2O_2 decomposition, and shock-heated H_2O/O_2 mixtures, and was found to be in very good agreement. In addition, the current mechanism has been validated against a wide range of more conventional H_2/O_2 kinetic targets, including ignition delay times, flow reactor species time-histories, laminar flame speeds, and burner-stabilized flame structures.

It is evident from this study that continued work on some elements of the H_2/O_2 sub-mechanism is still needed. In particular, accurate measurements of reaction rate coefficients are needed for several HO_2 reactions ($H + HO_2$ in particular), as well as for rate constant measurements and collisional efficiencies at high temperature and high pressure for HO_2 and H_2O_2 reactions. It is likely that as the commercial use of high-pressure reactors increases, the need for this information will become more and more critical.

Acknowledgments

This material is based upon work was supported by the National Science Foundation under Award No. 0649936, the Department of Energy, [Office of Basic Energy Sciences] under Award No. DE-FG02-88ER13857, and the Department of Energy [National Nuclear Security Administration] under Award No. NA28614.

Appendix A. Supplementary material

Supplementary data associated with this article can be found, in the online version, at doi:10.1016/j.combustflame.2010.10.002.

References

[1] C.K. Westbrook, F.L. Dryer, Prog. Energy Combust. Sci. 10 (1984) 1–57.
[2] M.A. Mueller, T.J. Kim, R.A. Yetter, F.L. Dryer, Int. J. Chem. Kinet. 31 (1999) 113–125.
[3] G. Del Álamo, F.A. Williams, A.L. Sánchez, Combust. Sci. Technol. 176 (2004) 1599–1626.
[4] J. Li, Z. Zhao, A. Kazakov, F.L. Dryer, Int. J. Chem. Kinet. 36 (2004) 566–575.
[5] M. Ó Conaire, H.J. Curran, J.M. Simmie, W.J. Pitz, C.K. Westbrook, Int. J. Chem. Kinet. 36 (2004) 603–622.
[6] A.A. Konnov, Combust. Flame 152 (2008) 507–528.
[7] I.Gy. Zsély, J. Zádor, T. Turányi, Proc. Combust. Inst. 30 (2005) 1273–1281.
[8] S.G. Davis, A.V. Joshi, H. Wang, F. Egolfopoulos, Proc. Combust. Inst. 30 (2005) 1283–1292.
[9] P. Saxena, F.A. Williams, Combust. Flame 145 (2006) 316–323.
[10] H. Sun, S.I. Yang, G. Jomaas, C.K. Law, Proc. Combust. Inst. 31 (2007) 439–446.
[11] Z. Hong, D.F. Davidson, E.A. Barbour, R.K. Hanson, Proc. Combust. Inst. 33 (2010), doi:10.1016/j.proci.2010.05.101.
[12] Z. Hong, A. Farooq, E.A. Barbour, D.F. Davidson, R.K. Hanson, J. Phys. Chem. A 113 (2009) 12919–12925.
[13] J. Troe, V.G. Ushakov, Phys. Chem. Chem. Phys. 10 (2008) 1–10.
[14] S.R. Sellevåg, Y. Georgievskii, J.A. Miller, J. Phys. Chem. A 113 (2009) 4457–4467.
[15] Z. Hong, S.S. Vasu, D.F. Davidson, R.K. Hanson, J. Phys. Chem. A 114 (2010) 5520–5525.
[16] Z. Hong, R.D. Cook, D.F. Davidson, R.K. Hanson, J. Phys. Chem. A 114 (2010) 5718–5727.
[17] S.R. Sellevåg, Y. Georgievskii, J.A. Miller, J. Phys. Chem. A 112 (2008) 5085–5095.
[18] X. Fernandes, K. Luther, J. Troe, V.G. Ushakov, Phys. Chem. Chem. Phys. 10 (2008) 4313–4321.
[19] G.P. Smith, D.M. Golden, M. Frenklach, N.W. Moriarty, B. Eiteneer, M. Goldenberg, C.T. Bowman, R.K. Hanson, S. Song, W.J. Gardiner Jr., V.V. Lissianski, Z. Qin, GRI-Mech 3.0, 1999. <http://www.me.berkeley.edu/gri-mech/>.
[20] J.V. Michael, J.W. Sutherland, L.B. Harding, A.F. Wagner, Proc. Combust. Inst. 28 (2000) 1471–1478.
[21] M.P. Burke, M. Chaos, F.L. Dryer, Y. Ju, Combust. Flame 157 (2010) 618–631.
[22] T.C. Germann, W.H. Willer, J. Phys. Chem. A 101 (1997) 6358–6367.
[23] C.B. Kretschmer, Investigation of Atomic Oxygen Recombination Rates, Aerojet-General Corporation Report 1611 (AFOSR-TR-59-62), AD 217008, May 1959.
[24] E. Goos, A. Burcat, B. Ruscic, Third Millennium Ideal Gas and Condensed Phase Thermodynamical Database for Combustion with Updates from Active Thermodynamical Tables, ANL-05/20 and TAE 960 Technion-IIT, Aerospeace Engineering, and Argonne National Laboratory, Chemistry Division, September 2005. <ftp://ftp.technion.ac.il/pub/supported/aetdd/thermodynamics/therm.dat> (accessed June 2010).
[25] J.T. Herbon, R.K. Hanson, D.M. Golden, C.T. Bowman, Proc. Combust. Inst. 29 (2002) 1201–1208.
[26] B. Ruscic, A.F. Wagner, L.B. Harding, R.L. Asher, D. Feller, D.A. Dixon, Y. Peterson, K.A. Song, X.M. Qian, C.Y. Ng, J.B. Liu, W.W. Chen, J. Phys. Chem. A 106 (2002) 2727–2747.
[27] B. Ruscic, R.E. Pinzon, M.E. Morton, N.K. Srinivasan, M.-C. Su, J.W. Sutherland, J.V. Michael, J. Phys. Chem. A 110 (2006) 6592–6601.
[28] B. Sirjean, E. Dames, D.A. Sheen, F.N. Egolfopoulos, H. Wang, D.F. Davidson, R.K. Hanson, H. Pitsch, C.T. Bowman, C.K. Law, W. Tsang, N.P. Cernansky, D.L. Miller, A. Violi, R.P. Lindstedt, A High-Temperature Chemical Kinetic Model of n-Alkane, Cyclohexane, and Methyl-, Ethyl-, n-Propyl and n-Butyl-Cyclohexane Oxidation at High Temperatures, September 2009. <http://www.melchior.usc.edu/JetSurF/JetSurF1.1> (accessed June 2010).
[29] W. Tsang, R.F. Hampson, J. Phys. Chem. Ref. Data 15 (1986) 1087–1279.
[30] G.L. Schott, Combust. Flame 21 (1973) 357–370.
[31] K.A. Pamidimukkala, G.B. Skinner, in: Thirteenth International Symposium on Shock Waves and Shock Tubes, SUNY, Albany, 1981, p. 585–592.
[32] P. Frank, Th. Just, Ber. Bunsen-Ges. Phys. Chem. 89 (1985) 181–187.
[33] N. Fujii, K.S. Shin, Chem. Phys. Lett. 151 (1988) 461–465.

[34] A.N. Pirraglia, J.V. Michael, J.W. Sutherland, R.B. Klemm, J. Phys. Chem. 93 (1989) 282–291.
[35] K.S. Shin, J.V. Michael, J. Chem. Phys. 95 (1991) 262–273.
[36] D.A. Masten, R.K. Hanson, C.T. Bowman, J. Phys. Chem. 94 (1990) 7119–7128.
[37] T. Yuan, C. Wang, C.-L. Yu, M. Frenklach, M.J. Rabinowitz, J. Phys. Chem. 95 (1991) 1258–1265.
[38] H. Du, J.P. Hessler, J. Chem. Phys. 96 (1991) 1077–1092.
[39] H. Yang, W.C. Gardiner, K.S. Shin, N. Fujii, Chem. Phys. Lett. 231 (1994) 449–453.
[40] C.-L. Yu, M. Frenklach, D.A. Masten, R.K. Hanson, C.T. Bowman, J. Phys. Chem. 98 (1994) 4770–4771.
[41] S. Ryu, S.M. Hwang, M.J. Rabinowitz, J. Phys. Chem. 99 (1995) 13984–13991.
[42] S.M. Hwang, Si-Ok Ryu, K.J. De Witt, M.J. Rabinowitz, Chem. Phys. Lett. 408 (2005) 107–111.
[43] R.W. Bates, D.M. Golden, R.K. Hanson, C.T. Bowman, Phys. Chem. Chem. Phys. 3 (2001) 2337–2342.
[44] J.V. Michael, M.-C. Su, J.W. Sutherland, J.J. Carroll, A.F. Wagner, J. Phys. Chem. A 106 (2002) 5297–5313.
[45] D.L. Baulch, C.T. Bowman, C.J. Cobos, R.A. Cox, Th. Just, J.A. Kerr, M.J. Pilling, D. Stocker, J. Troe, W. Tsang, R.W. Walker, J. Warnatz, J. Phys. Chem. Ref. Data 34 (2005) 757–1397.
[46] J.A. Miller, M.J. Pilling, J. Troe, Proc. Combust. Inst. 30 (2005) 43–88.
[47] C.J. Cobos, H. Hippler, J. Troe, J. Phys. Chem. 89 (1985) 342–349.
[48] J. Hahn, L. Kransnoperov, K. Luther, J. Troe, Phys. Chem. Chem. Phys. 6 (2004) 1997–1999.
[49] L.B. Harding, J. Troe, V.G. Ushakov, Phys. Chem. Chem. Phys. 2 (2000) 631–642.
[50] R. Atkinson, D.L. Baulch, R.A. Cox, J.N. Crowley, R.F. Hampson, R.G. Hynes, M.E. Jenkins, M.J. Rossi, J. Troe, Atoms. Chem. Phys. 4 (2004) 1461–1738.
[51] S.P. Sander, R.R. Friedl, D.M. Golden, M.J. Kurylo, R.E. Huie, V.L. Orkin, G.K. Moortgat, A.R. Ravishankara, C.E. Kolb, M.J. Molina, B.J. Finlayson-Pitts, JPL Publ. 02-25, 2003 (NASA-JPL, 2003).
[52] G.A. Pang, D.F. Davidson, R.K. Hanson, Proc. Combust. Inst. 32 (2009) 181–188.
[53] J.D. Mertens, D.M. Kalitan, A.B. Barrett, E.L. Petersen, Proc. Combust. Inst. 32 (2009) 295–303.
[54] C. Westbrook, Proc. Combust. Inst. 28 (2000) 1563–1577.
[55] J. Troe, Ber. Bunsen-Ges. Phys. Chem. 73 (1969) 946–952.
[56] E. Meyer, H.A. Olschewski, J. Troe, H.Gg. Wagner, Proc. Combust. Inst. 12 (1969) 345–355.
[57] H. Kijewski, J. Troe, Int. J. Chem. Kinet. 3 (1971) 223–235.
[58] Ch. Kappel, K. Luther, J. Troe, Phys. Chem. Chem. Phys. 4 (2002) 4392–4398.
[59] R. Zellner, F. Ewig, R. Paschke, G. Wagner, J. Phys. Chem. 92 (1988) 4184–4190.
[60] R. Forster, M. Frost, D. Fulle, H.F. Hamann, H. Hippler, A. Schlepegrell, J. Troe, J. Chem. Phys. 103 (1995) 2949–2958.
[61] D. Fulle, H.F. Hamann, H. Hippler, J. Troe, J. Chem. Phys. 105 (1996) 1001–1006.
[62] H. Hippler, J. Troe, Chem. Phys. Lett. 192 (1992) 333–337.
[63] H. Hippler, H. Neunaber, J. Troe, J. Chem. Phys. 103 (1995) 3510–3516.
[64] N.K. Srinivasan, M.-C. Su, J.W. Sutherland, J.V. Michael, B. Ruscic, J. Phys. Chem. A 110 (2006) 6602–6607.
[65] J.J. Schwab, W.H. Brune, J.G. Anderson, J. Phys. Chem. 93 (1989) 1030–1035.
[66] L.F. Keyser, J. Phys. Chem. 92 (1988) 1193–1200.
[67] R.-R. Lii, R.A. Gorse Jr., M.C. Sauer Jr., S. Gordon, J. Phys. Chem. 84 (1980) 819–821.
[68] R.A. Cox, J.P. Burrows, T.J. Wallington, Chem. Phys. Lett. 84 (1981) 217–221.
[69] D.L. Baulch, C.J. Cobos, R.A. Cox, C. Esser, P. Frank, Th. Just, J.A. Kerr, M.J. Pilling, J. Troe, R.W. Walker, J. Warnatz, J. Phys. Chem. Ref. Data 21 (1992) 411–734.
[70] D.L. Baulch, C.J. Cobos, R.A. Cox, P. Frank, G. Hayman, Th. Just, J.A. Kerr, T. Murrells, M.J. Pilling, J. Troe, R.W. Walker, J. Warnatz, J. Phys. Chem. Ref. Data 23 (1994) 847–1033.
[71] N.K. Srinivasan, J.V. Michael, Int. J. Chem. Kinet. 38 (2006) 211–219.
[72] V. Naudet, S. Javoy, C.E. Paillard, Combust. Sci. Technol. 164 (2001) 113–128.
[73] S. Javoy, V. Naudet, S. Abid, C.E. Paillard, Exp. Therm. Fluid Sci. 27 (2003) 371–377.
[74] M.S. Wooldridge, R.K. Hanson, C.T. Bowman, Int. J. Chem. Kinet. 26 (1994) 389–401.
[75] J.W. Sutherland, P.M. Patterson, R.B. Klemm, Proc. Combust. Inst. 23 (1991) 51–57.
[76] A. Lifshitz, J.V. Michael, Proc. Combust. Inst. 23 (1991) 59–67.
[77] R.R. Baldwin, R.W. Walker, J. Chem. Soc., Faraday Trans. 1 75 (1979) 140–154.
[78] W. Hack, A.W. Preuss, H.Gg. Wagner, K. Hoyermann, Ber. Bunsen-Ges. Phys. Chem. 83 (1979) 212–217.
[79] B.A. Thrush, J.P.T. Wilkinson, Chem. Phys. Lett. 84 (1981) 17–19.
[80] U.C. Sridharan, L.X. Qiu, F. Kaufman, J. Phys. Chem. 86 (1982) 4569–4574.
[81] L.F. Keyser, J. Phys. Chem. 90 (1986) 2994–3003.
[82] M.W. Slack, Combust. Flame 28 (1977) 241–249.
[83] K.A. Bhaskaran, M.C. Gupta, Th. Just, Combust. Flame 21 (1973) 45–48.
[84] G.B. Skinner, G.H. Ringrose, J. Chem. Phys. 42 (1965) 2190–2192.
[85] G.L. Schott, J.L. Kinsey, J. Chem. Phys. 29 (1958) 1177–1182.
[86] E.L. Petersen, D.F. Davidson, M. Röhrig, R.K. Hanson, in: B. Sturtevant, J.E. Shepherd, H.G. Hornung (Eds.), Proceedings of the 20th International Symposium on Shock Waves, Pasadena, California, 1995. pp. 941–946.
[87] B.L. Wang, H. Olivier, H. Grönig, Combust. Flame 133 (2003) 93–106.
[88] H. Li, Z.C. Owens, D.F. Davidson, R.K. Hanson, Int. J. Chem. Kinet. 40 (2008) 189–198.
[89] C.K. Wu, C.K. Law, Proc. Combust. Inst. 20 (1984) 1941–1949.
[90] O.C. Kwon, G.M. Faeth, Combust. Flame 124 (2001) 590–610.
[91] C.M. Vagelopoulos, F.N. Egolfopoulos, C.K. Law, Proc. Combust. Inst. 25 (1994) 1341–1347.
[92] D.R. Dowdy, D.B. Smith, S.C. Taylor, A. Williams, Proc. Combust. Inst. 23 (1990) 1341–1347.
[93] S.D. Tse, D.L. Zhu, C.K. Law, Proc. Combust. Inst. 28 (2000) 1793–1800.
[94] Chemkin-PRO, Reaction Design, San Diego, California, USA, 2008. <http://www.reactiondesign.com>.
[95] F.N. Egolfopoulos, C.K. Law, Proc. Combust. Inst. 23 (1990) 333–340.
[96] R.T.E. Hermanns, A.A. Konnov, R.J.M. Bastiaans, L.P.H. de Goey, Energy Fuels 21 (2007) 1977–1981.
[97] F.N. Egolfopoulos, C.K. Law, Combust. Flame 80 (1990) 7–16.
[98] G. Dixon-Lewis, M.M. Sutton, A. Williams, Proc. R. Soc. London, A 317 (1970) 227–234.
[99] J. Vandooren, J. Bian, Proc. Combust. Inst. 23 (1990) 341–346.
[100] A.A. Paletskii, L.V. Kuibida, T.A. Bolshova, O.P. Korobeinichev, R.M. Fristrom, Combust. Explos. Shock Waves 32 (1996) 245–250.